Time-Resolved Fluorescence Studies of Tomaymycin Bonding to DNA†

Qi Chen, Fahmida N. Chowdhury, Karol Maskos, and Mary D. Barkley*

Department of Chemistry, Louisiana State University, Baton Rouge, Louisiana 70803

Received December 29, 1993; Revised Manuscript Received May 16, 1994®

ABSTRACT: Tomaymycin is an antibiotic that reacts at guanine N2 in the minor groove of the DNA helix. The number and type of tomaymycin–DNA adducts present on natural sequence DNA were identified using time-resolved fluorescence spectroscopy. At low bonding density, only two discrete species were observed with lifetimes of 4.3 and 7.1 ns and relative amplitudes of 40% and 60%. These two lifetime species are proposed to represent either *R*5′ or *S*5′ and *S*3′ binding modes at the preferred bonding sequence 5′-AGA. *R* and *S* denote the configuration at C11 of tomaymycin, and 5′ and 3′ describe the orientation of the aromatic ring on the covalently modified strand. These two species were present over a range of solution conditions, including pH, nucleotide to drug ratio, DNA concentration, and DNA size. They have the same emission spectra, but slightly shifted absorption spectra. The weak temperature dependence of the fluorescence lifetimes presumably is due to the excited-state proton-transfer reaction that quenches tomaymycin fluorescence. The rate of formation of the longer lifetime species of DNA adduct is about twice as fast as that of the shorter lifetime species. Under saturating conditions, the fluorescence decay shows a bimodal lifetime distribution whether analyzed by least-squares assuming a Gaussian distribution model or by the maximum entropy method. The two groups of lifetimes are centered around 2–3 and 6–6.6 ns, reflecting multiple species on different bonding sequences.

Tomaymycin belongs to the group of pyrrolo[1,4]benzodiazepine antitumor antibiotics. The antitumor activity of these drugs is probably due to their ability to alkylate DNA (Hurley & Needham-VanDevanter, 1986). There are two chiral carbon centers in tomaymycin: C11 and C11a. C11a has an *S* configuration. The crystal structure of tomaymycin methyl ether shows an *R* configuration at C11 (Arora, 1981). In protic solvents, facile epimerization occurs at C11, producing a mixture of 11*R* and 11*S* diastereomers, whose relative populations depend on the solvent (Barkley et al., 1986). The epimerization mechanism is proposed to be nucleophilic substitution through an N10–C11 imine intermediate (Figure 1). DNA adducts presumably form by a similar mechanism, yielding an aminal bond from C11 of tomaymycin to N2 of guanine in the minor groove of B-form DNA (Petrusek et al., 1981; Barkley et al., 1986). The covalent linkage between tomaymycin C11 and guanine N2 was definitively established by ^{1}H NMR of the tomaymycin–d(CICGAATTCICG)$_2$ adduct (Boyd et al., 1990).

Despite the specific reaction with guanine, the pyrrolo[1,4]benzodiazepines do not alkylate all guanine residues in a DNA sequence with the same frequency (Hertzberg et al., 1986; Hurley et al., 1988; Pierce et al., 1993). The relative reactivity of a particular guanine depends upon the antibiotic as well as the proximal bases on the modified strand. The most preferred bonding sequence is 5′-PuGPu. Chemical footprinting with MPE Fe(II)[1] showed that the drugs protect a 3–4 base pair sequence (Hertzberg et al., 1986). The enhancement of MPE Fe(II) cleavage between some bonding sites suggests a drug-induced change in DNA conformation. Tomaymycin modified 29% of guanines in the 363 base pairs analyzed, with a sequence preference of 5′-PuGPu > 5′-PuGPy > 5′-PyGPu > 5′-PyGPy. More detailed sequence specificity was determined with an exonuclease III stop assay, where 30% of guanines in a 117 base pair restriction fragment were modified, most frequently at 5′-AGG = 5′-CGC > 5′-GGA > 5′-AGT (Hurley et al., 1988). Recently, a somewhat different sequence specificity was observed by UvrABC nuclease incision analysis; 80% of the guanines on the single labeled strand of a 238 base pair fragment were modified, primarily at 5′-AGA > 5′-GGC > 5′-TGC > 5′-AGC = 5′-GGA > 5′-AGG (Pierce et al., 1993).

There are four possible binding modes of pyrrolo[1,4]-benzodiazepines at guanine bases on DNA: an *R* or *S* configuration at C11 with the aromatic ring of the drug pointing toward the 3′ or 5′ end of the modified DNA strand. The binding mode of tomaymycin at 3 of the 16 possible 3 base pair sites has been determined by fluorescence, two-dimensional ^{1}H NMR, and molecular modeling studies of oligodeoxynucleotide adducts (Cheatham et al., 1988; Boyd et al., 1990; Wang et al., 1992; M. D. Barkley, K. Maskos, and Q. Chen, manuscript in preparation). The combination of these techniques is particularly powerful for determining the structure of drug–DNA complexes in the case of multiple binding modes (Remers et al., 1992). The fluorescence lifetimes of tomaymycin adducts with unique bonding sites appear to be more sensitive to the binding mode than to the flanking base sequence (Barkley et al., manuscript in preparation). The lifetimes group in two classes. The major lifetime component usually has a longer lifetime of 5–8 ns, and the minor component has a shorter lifetime of 1.5–5 ns. The longer lifetime in oligonucleotide adducts has been assigned to the 11*S* diastereomer and the shorter lifetime to the 11*R* diastereomer. The lifetime difference among binding modes has been attributed to excited-state proton transfer (Chen & Barkley, 1994; Barkley et al., manuscript in preparation).

† This work was supported by NIH Grant GM35009.

* Author to whom correspondence should be addressed.

® Abstract published in *Advance ACS Abstracts,* July 1, 1994.

[1] Abbreviations: Pu, purine; Py, pyrimidine; EDTA, ethylenediaminetetraacetic acid; MPE, methidiumpropyl-EDTA; TOM, tomaymycin; TME, tomaymycin 11-methyl ether; P/D, nucleotide to drug ratio; FWHM, full width at half-maximum; POPOP, 1,4-bis(5-phenyloxazol-2-yl)benzene; BBO crystal, β-BaB_2O_4; BBO, 2,5-bis(4-biphenylyl)oxazole; λ_{ex}, excitation wavelength; λ_{em}, emission wavelength; MEM, maximum entropy method.

0006-2960/94/0433-8719$04.50/0

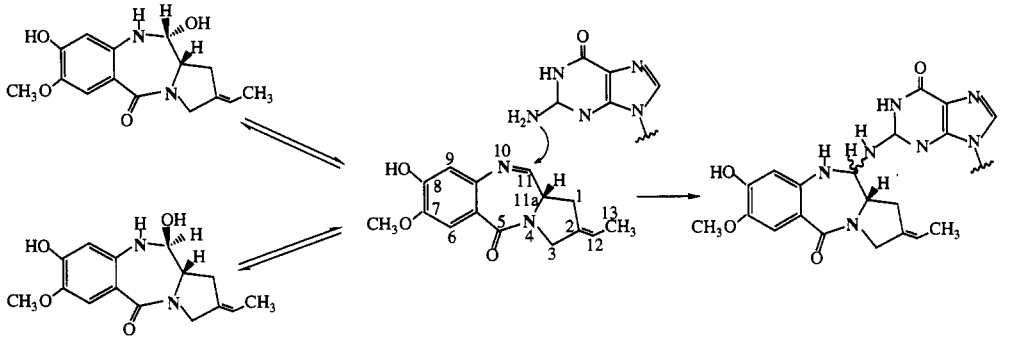

FIGURE 1: Proposed mechanism for the reaction of tomaymycin and DNA.

This paper examines the bonding of tomaymycin to calf thymus DNA, which has all 16 bonding sites. We use time-resolved fluorescence spectroscopy to identify the number and type of tomaymycin–DNA adducts present on natural sequence DNA. Analysis of the data by least-squares and maximum entropy methods in conjunction with simulation resolves the question of whether the fluorescence decay represents a few discrete lifetimes or a distribution of lifetimes in the range 2–8 ns. The effects of solution variables on the bonding reaction are determined. Finally, the observed lifetimes are assigned to specific binding modes and DNA bonding sites.

MATERIALS AND METHODS

Tomaymycin–DNA Adduct. (11*R*,11a*S*)-TME was a generous gift from Dr. M. Kohsaka, Fujisawa Pharmaceutical Co. (Osaka, Japan). Calf thymus DNA (Sigma type I) was purified by phenol extraction and was dialyzed into 10 mM phosphate buffer, pH 7.5, containing 0.1 M NaCl and 0.1 mM EDTA. DNA adducts were prepared as described previously (Barkley et al., 1991). The DNA concentration in adduct solutions was (0.2–2.5) × 10^{-3} M nucleotide. P/D ratios refer to the relative amounts of DNA and tomaymycin used in the reaction. The amount of tomaymycin actually bonded to DNA was determined by a difference method, in which the amount of unbound tomaymycin was measured by fluorescence after isobutyl alcohol extraction. At P/D = 1, all sites on DNA are saturated at 17–18 nucleotides per tomaymycin (Hurley, 1977; Barkley et al., manuscript in preparation). For the sample prepared at P/D = 100, 0.50 mL of adduct solution was extracted four times at 5 °C with equal volumes of isobutyl alcohol saturated with 10 mM phosphate buffer, pH 7.5. The isobutyl alcohol layers were combined and adjusted to a total volume of 5.00 mL at 25 °C. The fluorescence intensity was recorded at a 319-nm excitation wavelength and a 400-nm emission wavelength. Tomaymycin concentration was determined by comparison to a standard curve obtained under the same experimental conditions. At P/D = 100, the bonding density is 140 nucleotides per drug.

Unbound tomaymycin was removed prior to fluorescence experiments by three or four extractions with equal volumes of ethyl acetate. Traces of ethyl acetate were removed under vacuum. Photobleaching under laser light was completely eliminated by the scrupulous removal of oxygen. Adduct solution was placed in a 4 × 10 mm^2 cell (Helma, Jamaica, NY) sealed with the lubricated rubber stopper from a Vacutainer sterile tube (Becton Dickinson, Rutherford, NJ, No. 6381). The stopper was punctured by a needle above the solution. Oxygen gas was removed from the cell by alternative cycles of vacuum and argon for 0.5 h. High-purity argon gas was introduced through a copper line containing an Oxisorb gas purifier (Messer Griesheim, Valley Forge, PA). The stoppered cell was filled with argon after deoxygenation. Solutions remain oxygen free for at least 3 days when properly stoppered. Dissociation of tomaymycin from DNA is negligible up to 24 h at 5 °C. Both extraction and deoxygenation were performed in an ice bath. Sample absorbance at the lowest energy absorption maximum was <0.15 with a 10-mm path length.

Time-Resolved Fluorescence Measurements. Fluorescence lifetimes were measured on a Photochemical Research Associates time-correlated single photon counting instrument equipped with a Coherent 701-3 cavity-dumped DCM dye laser synchronously pumped by a mode-locked, frequency-doubled Quantronix 416 Nd-YAG laser. The output beam from the dye laser was frequency doubled by a BBO crystal and vertically polarized by a half-wave retarder. The excitation wavelength was selected with a three-plate birefringent filter. Emission was detected by a cooled Hamamatsu R955 photomultiplier, which was wired for an instrumental response of 360 ps FWHM (McMahon et al., 1992). The emission polarizer was set at 54.7° in order to eliminate anisotropic effects. The emission (8-nm bandpass) wavelength was selected by an Instruments SA H-10 monochromator. Data acquisition was controlled by a Macintosh IIcx computer using a program based on the LabVIEW software package (Stryjewski, 1991). Sample temperature was controlled by a circulating bath at 5 °C unless indicated otherwise.

Fluorescence decays from the sample and reference fluorophore were acquired contemporaneously to (2.5–5) × 10^4 counts in the peak channel ((5–10) × 10^6 total counts). The counting rate was usually about 6 kHz; the excitation rate was 760 kHz. Decay curves were stored in 512 or 1024 channels of 0.06 or 0.03 ns/channel, respectively. Solutions of quenched POPOP (Fluka, Buehs, Switzerland) in 75% ethanol and 0.8 M KI (containing a trace of sodium thiosulfate to retard I_3^- formation) or BBO in ethanol were used as reference fluorophore. A lifetime of quenched POPOP of about 0.21 ns and a lifetime of BBO of about 1.24 ns were determined in separate experiments using anthracene in ethanol as the monoexponential standard. Data sets at high P/D ratio as well as different pH, DNA concentration, wavelength, chain length, and temperature were collected to about 9 × 10^3 counts in the peak channel (about 6 × 10^5 total counts) using a nitrogen flash lamp, as described elsewhere (Barkley et al., manuscript in preparation).

Data Analysis. Fluorescence decay curves were analyzed by reference deconvolution (Kolber & Barkley, 1986) assuming discrete and distributed decay models. The discrete lifetime model is described by

$$I(\lambda_{ex}, \lambda_{em}; t) = \sum_{i=1}^{n} \alpha_i(\lambda_{ex}, \lambda_{em}) \exp(-t/\tau_i) \qquad (1)$$

where $I(\lambda_{ex}, \lambda_{em}; t)$ is the fluorescence intensity, and the

fluorescence lifetimes τ_i and relative amplitudes $\alpha_i(\lambda_{ex}, \lambda_{em})$ are the fitting parameters. Single curve and multiple curve analyses were performed using a global nonlinear least-squares fitting program (Beechem, 1989). The lifetimes are usually linked in multiple curve analyses. The reference lifetime is fixed at a known value determined separately. The success of the fit is judged by statistical parameters: reduced chi-square (χ_r^2), weighted residuals, and the autocorrelation function of the weighted residuals.

The fluorescence decay curves measured at different temperatures were analyzed according to eq 1, with the lifetimes τ_i replaced by an Arrhenius expression:

$$\tau_i^{-1} = k_{oi} + A_i \exp(-E_i/RT) \quad (2)$$

where the amplitudes α_i, temperature-independent rate constants k_{oi}, frequency factors A_i, and activation energies E_i are the fitting parameters. The values of k_{oi}, A_i, and E_i at different temperatures are linked in the global analysis.

The distribution model is described by

$$I(\lambda_{ex}, \lambda_{em}; t) = \int_0^\infty \alpha(\tau) \exp(-t/\tau)\, d\tau \quad (3)$$

where $\alpha(\tau)$ is the spectrum of lifetimes τ. Two types of distribution analyses were performed: (1) $\alpha(\tau)$ is assumed to have a Gaussian distribution, and (2) $\alpha(\tau)$ is allowed to take the form most compatible with the experimental data by maximizing the Skilling–Jaynes entropy function (Jaynes, 1983; Livesey & Skilling, 1985).

In the Gaussian distribution model, the function $\alpha(\tau)$ is given by

$$\alpha(\tau) = \sum_{i=1}^{n} [\alpha_i/(\sigma_i(2\pi)^{1/2})] \exp[-(\tau - \tau_{oi})^2/(2\sigma_i^2)] \quad (4)$$

where $n = 1$ and $n > 1$ represent unimodal and multimodal Gaussian distributions, respectively. The mean lifetimes τ_{oi}, standard deviations σ_i, and peak areas α_i are the fitting parameters. In order for $\alpha(\tau)$ to be a valid probability density function, α_i must be normalized so that the total area under the function $\alpha(\tau)$ is unity, $\sum_{i=1}^{n} \alpha_i = 1$. This distribution analysis is also globalized in the same way as the discrete analysis. The integration in eq 3 is carried out numerically (Beechem, 1989). Although in principle multiple components are allowed, in practice it is almost impossible to resolve more than two. Attempts to use three or more components result in high sensitivity to the initial guess, which follows from the large number of fitting parameters and the presence of local minima. This is a disadvantage of the model fitting approach, in addition to the potentially more serious problem of prescribing the type of distribution. The Beechem global program features three types of distributions: Gaussian, Lorentzian, and uniform. However, expansion of the repertoire of probability density functions does not give full flexibility to the shape of the function $\alpha(\tau)$. These limitations are overcome by using an entirely different approach to data analysis, the so-called maximum entropy method (MEM) (Gull & Skilling, 1984; Skilling & Bryan, 1984).

The important advantage of MEM is that the shape of the function $\alpha(\tau)$ is not predetermined. The analysis automatically results in the inclusion of as many peaks (called "modes" in Gaussian analysis jargon) as are necessary for the best fit to the data. The basic model for the decay function is still the same as that in eq 3, but the shape of $\alpha(\tau)$ is determined from the experimental data. The best fit is approached by maximizing the Skilling–Jaynes entropy function:

$$S(\alpha) = \int_0^\infty \{\alpha(\tau) - m(\tau) - \alpha(\tau) \log[\alpha(\tau)/m(\tau)]\}\, d\tau \quad (5)$$

where $m(\tau)$ is the initial guess, usually set to a flat distribution in the absence of a priori knowledge about the distribution. The FAME5 program replaces the integrations in eqs 3 and 5 by summations of up to 250 lifetime values equally spaced in a logarithmic or linear scale. The entropy, S, is maximized together with minimization of χ_r^2 (the normalized overall fitting error) for the fit to eq 3. Thus, the conventional distribution and MEM analyses are similar in that both use the same fitting function and minimize χ_r^2 as in any nonlinear least-squares fitting technique. They differ in that MEM determines the density function $\alpha(\tau)$ by maximizing the entropy function $S(\alpha)$, whereas conventional distribution analysis specifies the form of the distribution. The one limitation of the current version of FAME5 is that it is not globalized. However, a global version may be available in the near future (J.-C. Brochon, personal communication).

The broadness of a peak in FAME5 is described by the dispersion, D

$$D = \{[\sum_{i=j}^{k} \alpha(i)\{\tau(i) - \bar{\tau}\}^2]/\sum_{i=j}^{k} \alpha(i)\}^{1/2} \quad (6a)$$

where the average lifetime $\bar{\tau}$ is

$$\bar{\tau} = [\sum_{i=j}^{k} \alpha(i)\tau(i)]/\sum_{i=j}^{k} \alpha(i) \quad (6b)$$

and j and k define the range of the peak. The dispersion D is the equivalent of the estimated standard deviation σ in the case of a Gaussian distribution. The relative amplitude α_i of a peak is determined from its relative area.

Fluorescence decay data containing Gaussian noise were simulated by convolution of the desired decay model with an experimental lamp profile in the Beechem global program. One-, two-, and three-exponential decays were generated using eq 1. Unimodal and bimodal Gaussian distributions were generated using eqs 3 and 4.

Bonding Kinetics. The formation of DNA adduct was monitored by fluorescence lifetime measurements with flash lamp excitation as described elsewhere (Barkley et al., manuscript in preparation). Decay curves were acquired at different times after mixing TME and DNA and were deconvoluted by global analysis assuming three exponentials. Rate constants were determined from changes in relative amplitudes of the lifetime components as a function of time. The reaction

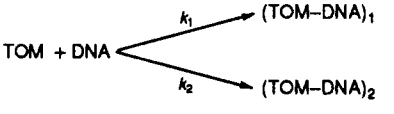

was carried out at P/D = 100 or a 25-fold excess of potential DNA bonding sites. The hydrolysis of tomaymycin methyl ether to form tomaymycin is fast compared to the reaction with DNA. Therefore, at early times in the reaction where there is negligible dissociation of adduct, pseudo-first-order kinetics can be assumed. The apparent pseudo-first-order rate constants were $k_1' = k_1[\text{DNA}]_o$ for the shorter lifetime species, $k_2' = k_2[\text{DNA}]_o$ for the longer lifetime species, and $k_f' = k_f[\text{DNA}]_o$ for free tomaymycin, where $k_f' = k_1' + k_2'$ and $[\text{DNA}]_o = 1 \times 10^{-3}$ M nucleotide. The pseudo-first-order rate constant k_f' was determined from the slope of the

linear portion of a plot of $-\ln \alpha_f$ vs t, where α_f is the relative amplitude of the free drug decay. The pseudo-first-order rate constant k_i' for species i was obtained by a least-squares fit of the amplitude α_i to

$$\alpha_i = (k_i'/k_f')[1 - \exp(-k_f't)] \quad (7)$$

The value of k_f' was fixed in the analysis of α_i. Arrhenius parameters were calculated from the temperature dependence of the apparent bimolecular rate constant k_i:

$$k_i = A \exp(-E_a/RT) \quad (8a)$$

$$A = (k_B T/h) \exp(1 + \Delta S^*/R) \quad (8b)$$

where E_a is the activation energy, ΔS^* is the activation entropy, k_B is the Boltzmann constant, and h is the Planck constant.

RESULTS

Model Discrimination. There are 16 DNA bonding sites on natural DNA sequences and four binding modes at each site. If we assume that all species of adduct are fluorescent, there is a total of 64 possible tomaymycin–DNA adducts with lifetimes in the range 1.5–8 ns. In order to determine the number and type of adducts present on DNA, we need to establish criteria for distinguishing decay models. It is well known that frequently more than one model will fit the experimental data equally well. It can be a difficult, sometimes impossible, task to isolate the true decay model under such circumstances. Simulation studies are a very useful tool to validate or refute particular lifetime models. Therefore, we performed extensive simulation studies to gain insight into the analysis of discrete and distributed decay models with lifetimes in the range of interest for tomaymycin–DNA adducts. A summary of the major conclusions follows.

(1) Simulated Discrete Models. Increasing the model order in a discrete analysis improves χ_r^2 until redundancy of the model becomes obvious. A Gaussian distribution analysis always gives a good fit with the same mean lifetimes τ_{oi} as the discrete lifetimes τ_i and poorly determined standard deviations σ_i. For example, a simulated 3.5-ns single exponential gives an excellent fit to a unimodal Gaussian with $\tau_o = 3.5$ ns and $\sigma = 0.15$–0.20. It is practically impossible to distinguish between a triple exponential and a wide unimodal Gaussian without the help of a model-free approach, such as MEM. Simulated data for discrete models also fit quite well to continuous distributions by MEM. However, in such cases the dispersions of the modes typically are rather small, and the number of peaks in the recovered $\alpha(\tau)$ distribution matches the actual number of components in the discrete model.

(2) Simulated Unimodal Gaussian Models. A discrete analysis gives a good χ_r^2 value if the standard deviation of the distribution is small: $\sigma = 0.01$–0.15 ns. As σ becomes larger, higher order discrete models give better fits. However, the recovered lifetimes may be quite different between double- and triple-exponential models. A wide unimodal Gaussian gives acceptable fits to both uni- and bimodal Gaussian models, particularly for noisy data, because the standard deviation is so poorly determined in the analysis.

(3) Simulated Bimodal Gaussian Models. A double-exponential analysis gives acceptable χ_r^2 values of about 1.3–1.5. As σ becomes larger, a triple exponential may give an acceptable fit and a new set of recovered parameters.

It is preferable to recover the lifetime distribution without having to assume a specific form in the analysis program. We therefore turned to the maximum entropy method for fluorescence data analysis (Livesey & Brochon, 1987). Presently, we are using the MEM program in conjunction with other deconvolution programs to help distinguish various models that fit our data equally well. In this paper, Gaussian distribution and MEM analyses are used in a cooperative, not competitive fashion; both methods are also aided by extensive simulation studies to explore the probable behavior of specific models. Here we outline our strategy for model discrimination gleaned from simulation studies.

(1) We routinely analyze all data with both discrete and distribution models. If the data fit substantially better to one model, as judged by a lower χ_r^2 value or more random autocorrelation function or both, then the other is discarded.

(2) If the distribution model fits equally well or better than the discrete model, we try to confirm the distribution model by discrete analyses with increasing numbers of components. Simulation studies have shown that the χ_r^2 value for distributed lifetime data analyzed by discrete models keeps improving with increasing numbers of components in the analysis. Therefore, if the fit to higher order discrete models fails to show progressive improvement, then the distribution model may be discarded.

(3) If the data fit well to a bimodal Gaussian model but MEM shows only one peak, we incline toward a unimodal distribution of non-Gaussian shape. If the data fit equally well to the double-exponential and bimodal Gaussian models, and the presence of two peaks is verified by the MEM analysis, then we carry out simulation studies in an attempt to reach a conclusion. Typically, we would simulate a biexponential decay with the same amplitudes and lifetimes as the values recovered from discrete analysis of the experimental data and analyze the simulated data with various distribution models. We would then compare the standard deviation or dispersion obtained from these distribution analyses to the experimental values. If they are similar, then the distribution model is discarded altogether. Obviously, a known discrete data set producing the same results as our experimental data for a distribution analysis renders the distribution results meaningless.

(4) On the other hand, if the standard deviation or dispersion for a distribution analysis of the experimental data were substantially larger than the value obtained from the discrete simulated data, then we would choose the distribution model over the discrete model. As to the actual shape of the density function $\alpha(\tau)$, the MEM result is more trustworthy. In our experience, a data set that truly represents a Gaussian distribution of lifetimes yields the same values of the decay parameters for the Gaussian and MEM analyses, whereas the fit to a discrete model gives a larger χ_r^2 value.

Lifetime Model for the Tomaymycin–DNA Adduct. Two extreme examples of tomaymycin–DNA adducts were studied. At P/D = 100 there is a large excess of DNA bonding sites, and the drug will react preferentially at preferred bonding sequences. At P/D = 1 the DNA is saturated with tomaymycin, and less preferred bonding sequences will also be occupied. Fluorescence decays were measured at various excitation and emission wavelengths at 5 °C. Unreacted tomaymycin was removed immediately prior to experiments by the extraction of adduct solutions. Decay curves were deconvoluted in single and multiple curve analyses.

For the tomaymycin–DNA adduct prepared at P/D = 100, 25 decay curves were acquired at 318-, 320-, 323-, and 333-nm excitation wavelengths and 400-, 410-, 415-, and 420-nm emission wavelengths. Global analysis linking the lifetimes gave χ_r^2 values of 1.3–1.5 and randomly oscillating autocorrelation functions for fits to a double exponential and to

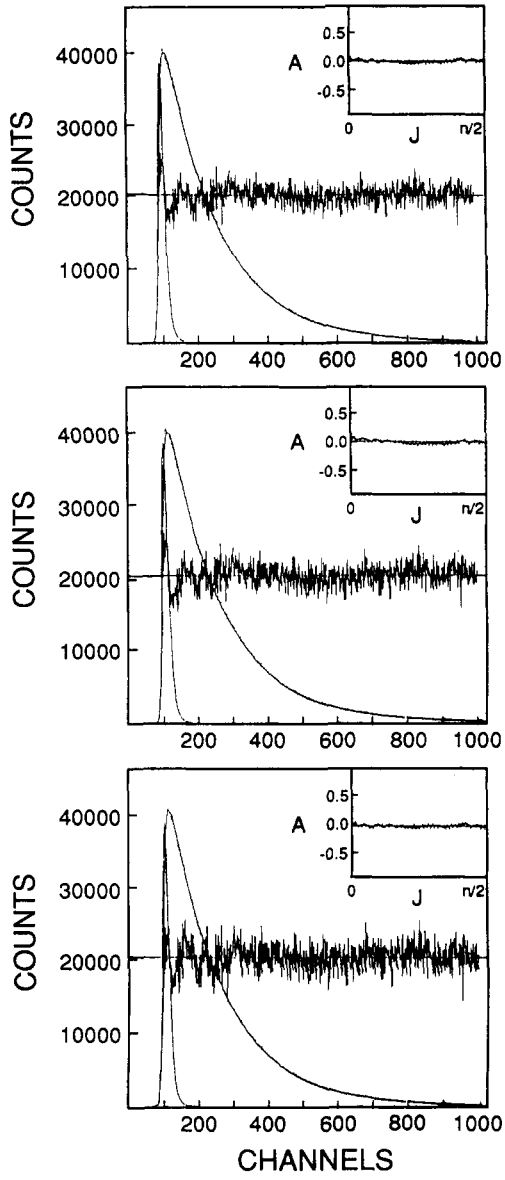

FIGURE 2: Global analysis of the fluorescence decay of tomaymycin–DNA adduct at pH 7.5, P/D = 100, 5 °C (λ_{ex} = 333 nm, λ_{em} = 410 nm, 0.037 ns/channel). The left curve is reference decay, points are sample decay, and smooth curve through the points is the best fit to the following: (top) double-exponential model, $\alpha_1 = 0.41$, $\tau_1 = 4.3$ ns, $\alpha_2 = 0.59$, $\tau_2 = 7.1$ ns, local $\chi_r^2 = 1.4$; (middle) unimodal Gaussian distribution, $\tau = 5.8$ ns, $\sigma = 1.4$ ns, local $\chi_r^2 = 1.5$; (bottom) bimodal Gaussian distribution, $\alpha_1 = 0.25$, $\tau_1 = 2.7$ ns, $\sigma_1 = 0.13$ ns, $\alpha_2 = 0.75$, $\tau_2 = 6.3$ ns, $\sigma_2 = 0.23$ ns, local $\chi_r^2 = 1.5$. Weighted residuals and the autocorrelation function of the residuals (inset) are also shown.

unimodal and bimodal Gaussian distributions (Figure 2; Table 1). Increasing the number of components in the discrete analysis did not improve the fit. The fluorescence lifetimes were independent of both the excitation and emission wavelengths; the lifetimes obtained from single curve analyses were within 0.3 ns of the global results. The relative amplitudes were also independent of the emission wavelength, but slightly dependent on the excitation wavelength. Figure 2 shows the double-exponential and unimodal and bimodal Gaussian fits. The discrete analysis gave lifetimes $\tau_1 = 4.3$ ns and $\tau_2 = 7.1$ ns, compared to mean lifetimes of 2.7 and 6.3 ns for the two narrow peaks of the bimodal Gaussian distribution. A much broader unimodal Gaussian distribution gave a slightly lower χ_r^2 value than the bimodal distribution, possibly because the two discrete lifetimes are very close. From these results alone, it is difficult to choose between the double-exponential and unimodal Gaussian models.

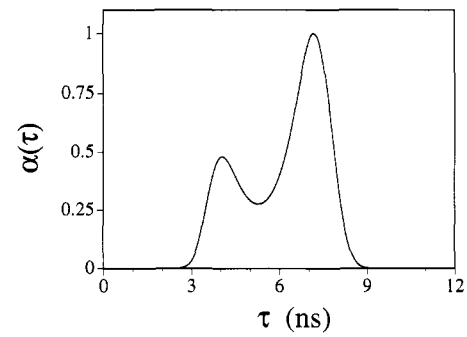

FIGURE 3: Lifetime distribution of tomaymycin–DNA adduct at P/D = 100 from MEM. Analysis was carried out in logarithmic space; results are displayed on a linear scale (λ_{ex} = 318 nm, λ_{em} = 410 nm). Normalized areas of relative amplitude under the peak and average lifetimes are $\alpha_1 = 0.44$, $\bar{\tau}_1 = 4.3$ ns, $D_1 = 0.54$ ns, $\alpha_2 = 0.56$, $\bar{\tau}_2 = 6.9$ ns, $D_2 = 0.73$ ns, $\chi_r^2 = 1.33$.

Two overlapping peaks at about 4 and 7 ns were resolved by MEM in single curve analyses (Figure 3). These lifetimes are very close to the values obtained for the double-exponential model. The dispersions are 0.4–0.8 ns. However, synthetic data generated for a discrete model having these decay parameters gave the same two peaks with dispersions comparable to the experimental data (Figure 4). Other simulated double-exponential decays were also analyzed to see how well MEM recovers parameters from data with 3.5 × 10^4 counts in the peak. Two distinct peaks were observed for the 4- and 7-ns double exponential, where $\tau_2/\tau_1 = 1.75$. The two peaks merge into a broader peak as τ_2/τ_1 decreases and finally become one peak at $\tau_2/\tau_1 = 1.2$ (Figure 4). Therefore, the MEM analysis argues strongly for the double-exponential model for the tomaymycin–DNA adduct. The unimodal Gaussian distribution model was discarded because two peaks were obtained by MEM.

For tomaymycin–DNA adduct prepared at P/D = 1, 10 decay curves were acquired at 330-, 333-, and 337-nm excitation wavelengths and 400-, 405-, and 410-nm emission wavelengths and were analyzed by the strategy outlined above. Unlike the case for P/D = 100, increasing the number of components in the discrete model improved the fit up to a triple exponential (Table 1). Fits to four and five components depended on an initial guess, with no improvement in global χ_r^2 values. This suggested the presence of a distribution of lifetimes. The fit to a unimodal Gaussian distribution was unacceptable. The bimodal Gaussian distribution gave a much better χ_r^2 value, pointing to the presence of at least two groups of lifetimes. The trimodal Gaussian distribution gave physically unreasonable results and no improvement in χ_r^2. MEM recovered two peaks at about 1.8 and 6.0 ns with dispersion values of 0.43 and 0.97 ns, respectively (Figure 5). MEM analysis of a double exponential simulated with these decay parameters returned two narrow peaks with the same lifetimes and amplitudes, but dispersion values of only 0.11 and 0.17 ns. In addition, a triple-exponential decay was simulated using the parameters obtained in the three-component fit of the experimental data (Table 1) and was analyzed using MEM. The MEM analysis gave one narrow peak at 1.6 ns with dispersion of 0.26 ns and a broad peak at 6.7 ns with dispersion of 1.17 ns. The broad peak contained a distinct shoulder at about 4 ns, clearly indicating the presence of the third lifetime. Such a shoulder was never seen in MEM analyses of the experimental data. Therefore, we conclude that the two peaks from MEM analysis of the experimental data represent two groups of distributed lifetimes rather than two or three discrete lifetimes. The average lifetimes were independent of both excitation and emission wavelengths. However, the relative

Table 1: Analysis of Time-Resolved Fluorescence Data for Tomaymycin–DNA Adduct[a]

analysis method	α_1(333 nm)[b]	τ_1 (ns)[c]	σ_1 (ns)[d]	α_2(333 nm)[b]	τ_2 (ns)[c]	σ_2 (ns)[d]	τ_3 (ns)	χ_r^2
P/D = 100 least-squares[e]								
single		6.0						11.5
double	0.41 ± 0.02	4.3 ± 0.3			7.1 ± 0.2			1.5
unimodal		5.8	1.4					1.3
bimodal	0.25	2.7	0.13		6.3	0.23		1.5
MEM[f]	0.40 ± 0.05	4.2 ± 0.4	0.55 ± 0.12		7.0 ± 0.4	0.75 ± 0.09		1.4
P/D = 1 least-squares[g]								
single		5.8						20.9
double	0.29 ± 0.02	2.2 ± 0.1			6.4 ± 0.1			1.7
triple	0.18 ± 0.02	1.6 ± 0.1		0.28 ± 0.01	4.4 ± 0.6		6.7 ± 0.3	1.5
unimodal		5.3	1.9					3.4
bimodal	0.54 ± 0.03	3.3	2.2		6.6	0.01		1.6
MEM[h]	0.25 ± 0.03	1.8 ± 0.1	0.43 ± 0.09		6.0 ± 0.1	0.97 ± 0.14		1.5

[a] pH 7.5, 5 °C. [b] Amplitude for discrete models; area under the peak for Gaussian distributions and MEM. [c] Lifetimes for discrete models are obtained from global analysis. These lifetimes are identical to the average values from single curve analyses. Errors are standard deviations from the single curve analyses. Mean lifetimes for Gaussian distributions are obtained from global analysis. Average lifetimes and standard deviations for MEM are obtained from single curve analyses. [d] Standard deviation in Gaussian distribution analysis; dispersion in MEM analysis. [e] Global analysis of 25 decay curves. [f] Single curve analyses of 25 decay curves. [g] Global analysis of 10 decay curves. [h] Single curve analyses of 10 decay curves.

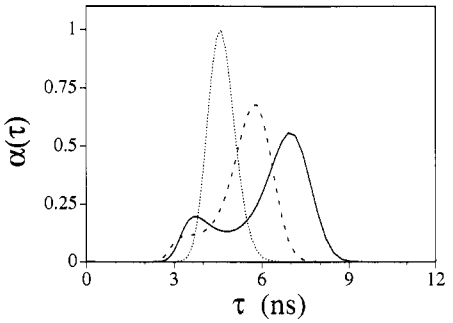

FIGURE 4: Lifetime distributions of simulated double-exponential decays analyzed by MEM. Amplitude ratio $\alpha_2/\alpha_1 = 3/2$; $\tau_1 = 4$ ns. Lifetime ratios τ_2/τ_1 used in simulation and recovered dispersions are (—) $\tau_2/\tau_1 = 1.75$, $D_1 = 0.49$ ns, $D_2 = 0.85$ ns; (– – –) $\tau_2/\tau_1 = 1.5$, $D = 1.02$ ns; (· · ·) $\tau_2/\tau_1 = 1.2$, $D = 0.46$ ns.

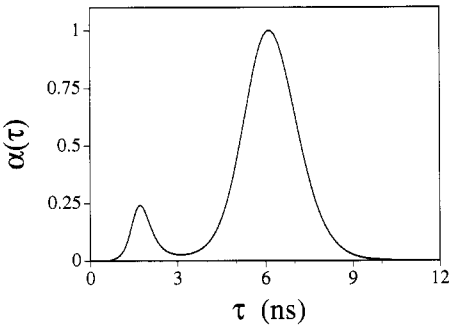

FIGURE 5: Lifetime distribution of tomaymycin–DNA adduct at P/D = 1 from MEM. Analysis was carried out in logarithmic space; results are displayed on a linear scale (λ_{ex} = 333 nm, λ_{em} = 400 nm). Normalized areas of relative amplitude under the peak and average lifetimes are $\alpha_1 = 0.25$, $\bar{\tau}_1 = 1.8$ ns, $D_1 = 0.43$ ns, $\alpha_2 = 0.75$, $\bar{\tau}_2 = 6.0$ ns, $D_2 = 1.01$ ns, $\chi_r^2 = 1.41$.

amplitudes of the two peaks varied with excitation wavelength. For example, α_1 decreased from 28% at 330 nm to 22% at 337 nm. This is much greater than the 2% change observed between 313 and 337 nm for the adduct prepared at P/D = 100 (Table 2), presumably reflecting more heterogeneous bonding species.

The Gaussian and MEM analyses both indicate bimodal lifetime distributions for the experimental data at P/D = 1. The two methods gave somewhat different decay parameters with similar χ_r^2 values. The bimodal Gaussian distribution looks like one broad peak at 3.3 ns, with a standard deviation of 2.2 ns and a discrete lifetime of 6.6 ns, whereas the MEM profile has two broad peaks at 1.8 and 6.0 ns (Table 1). Synthetic data were generated for a bimodal Gaussian

Table 2: Effect of Conditions on Tomaymycin–DNA Adduct[a]

P/D	pH	[DNA] (mM)	size[b]	λ_{ex} (nm)	α_1[c]
100	6.4	2.5	high MW	313	0.35
500					0.36
1000					0.34
100	6.4	2.5	high MW	337	0.38[d]
	7.5				0.37[d]
	8.9				0.34[d]
100	7.5	0.25	high MW	337	0.33
		0.63			0.34
		1.3			0.34
		2.5			0.34
100	7.5	2.5	high MW	313	0.34
				337	0.32
				350	0.29
100	7.5		65–110 bp	350	0.41
			25–36 bp		0.44
			<18 bp		0.41
			5–140 bp		0.44

[a] Global analysis assuming a double-exponential model of data acquired at 5 °C: $\tau_1 = 3.7$ ns, $\tau_2 = 6.7$ ns. pH dependence data were acquired at 25 °C and analyzed separately: $\tau_1 = 3.1$ ns, $\tau_2 = 5.6$ ns. [b] High MW is highly polymerized calf thymus DNA. Short DNA fragments were prepared by sonication of salmon sperm DNA and fractionation by gel chromatography. [c] Estimated standard deviation ±0.02. [d] Experiments at 25 °C.

distribution model with the decay parameters obtained from the MEM analysis. Bimodal Gaussian distribution and MEM analyses recovered the input decay parameters. Synthetic data were also generated for a bimodal Gaussian distribution with a single broad peak at 3.3 ns and a discrete lifetime of 6.6 ns. The bimodal Gaussian distribution analysis recovered either the input parameters or two broad peaks, depending on the initial guess. MEM analysis returned two broad peaks with shorter lifetimes than the input parameters, which is similar to the results from the experimental data. By combining the Gaussian and MEM results, the major group of lifetimes appears centered at 6–6.6 ns and the minor at around 2–3 ns. However, the profile of the distribution is uncertain.

Experimental Conditions. Tomaymycin appears to form only two species of adduct on natural sequence DNA at P/D = 100, pH 7.5, and 5 °C. We surveyed a variety of experimental conditions and found no evidence for additional species. A large data set containing almost 200 decay curves was measured at different excitation and emission wavelengths, P/D ratio, pH, DNA concentration, and DNA chain length. A χ_r^2 value of 1.1 was obtained for the global fit to a triple-exponential model with the lifetimes linked: two components

for tomaymycin–DNA adduct and one component for free drug. The two lifetimes for the DNA adduct were $\tau_1 = 3.7$ ns and $\tau_2 = 6.7$ ns. Note that these lifetimes are shorter than the values reported in Table 1. The reason appears to be numerical. These decay curves were fit to three exponentials because a 1-ns free drug component was always present, whereas the lifetime values in Table 1 were recovered from double-exponential fits of data from extracted samples. It can be easily verified that the mean lifetimes remain the same in all cases. Simulation studies suggest that if the free drug component has a very small preexponential factor, the double-exponential analysis will yield slightly greater lifetime values than the triple-exponential analysis. The insensitivity of the fluorescence lifetimes to experimental variables indicates that the same two species of DNA adduct are present under all conditions. However, there were small changes in the relative amplitudes of the two components under some conditions (Table 2). In the case of ground-state heterogeneity, the amplitudes of a fluorescence decay are proportional to the molar extinction spectrum, fluorescence emission spectrum, radiative lifetime, and concentration of the different species. As above, the amplitudes were independent of the emission wavelength, indicating that the emission spectra of the two lifetime components are the same. On the other hand, the amplitudes of the minor lifetime component decreased slightly relative to the major lifetime component with increasing excitation wavelength, signifying that the absorption spectrum of the minor component is blue-shifted relative to the spectrum of the major component. This is consistent with previous results showing that different species of tomaymycin–DNA adduct have the same emission spectra, but slightly shifted absorption spectra (Barkley et al., 1986).

The relative amplitudes of the two components are constant at P/D ratios ≥100. Such ratios are well above the saturation level of 17 nucleotides per drug in calf thymus DNA (Barkley et al., manuscript in preparation). At P/D = 100 the relative concentrations of the two species of DNA adduct are not affected by DNA concentration over a 10-fold range or by pH in the range 6–9. The relative concentration of the minor species of DNA adduct is 12–14% higher in short fragments of sonicated salmon sperm DNA (42% GC) than in highly polymerized calf thymus DNA (43% GC). Apparently, short DNA sequences favor formation of the minor species of DNA adduct.

Temperature Dependence. The fluorescence lifetimes of tomaymycin–DNA adducts are weakly temperature dependent. Fluorescence decay curves were acquired at 5° intervals from 5 to 25 °C at 313-, 337-, and 355-nm excitation wavelengths and at 420-nm emission wavelength. The temperature data set was deconvoluted globally with the temperature-independent rates k_{oi}, frequency factors A_i, and activation energies E_i linked in the analysis. The double-exponential fit gave a global χ_r^2 of 1.2. The temperature-independent rates and activation energies were the same for both components. Linking these parameters in the global analysis gave $k_{oi} = 1.1 \times 10^8$ s^{-1} and $E_i = 21$ kJ/mol. The frequency factors were different: $A_1 = 1.1 \times 10^{12}$ s^{-1} for the shorter lifetime component and $A_2 = 3.5 \times 10^{11}$ s^{-1} for the longer lifetime component. Intersystem crossing and excited-state proton transfer are the major nonradiative processes for tomaymycin (Barkley et al., manuscript in preparation; Chen & Barkley, 1994). The temperature-independent processes are the same for both components, while the temperature-dependent proton transfer rates are different due to different binding modes in the two components. The temperature-independent rate k_{oi} is usually the sum of the radiative k_r and

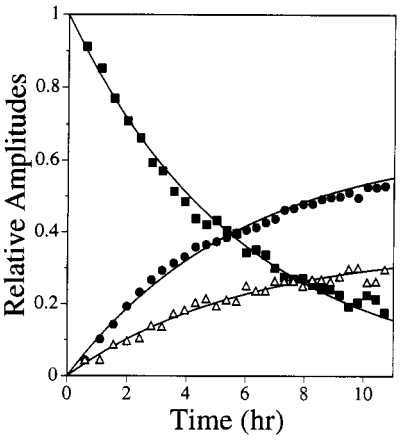

FIGURE 6: Kinetics of formation of tomaymycin–DNA adduct (λ_{ex} = 313 nm, λ_{em} = 420 nm, pH 7.5, 10 °C, [DNA] = 1 × 10^{-3} M, P/D = 100). Results from global fit to three exponentials ($\chi_r^2 = 1.1$): (■) free drug; (△) 3.74-ns component; (●) 6.57-ns component. Smooth curves are the best fits using eq 7.

Table 3: Kinetics Data for Formation of Tomaymycin–DNA Adduct[a]

species	k_i (M^{-1} s^{-1})[b]	E_a (kJ/mol)	$A \times 10^{-6}$ (M^{-1} s^{-1})	$\Delta S^{\ddagger}$ (J K^{-1} mol^{-1})
free drug	0.219	39	3.48	−127
short lifetime	0.078	40	1.90	−124
long lifetime	0.141	39	2.05	−131

[a] pH 7.5, [DNA] = 1 × 10^{-3} M, P/D = 100. [b] 10 °C.

intersystem crossing k_{isc} rates. Taking $k_r = (5–8) \times 10^7$ s^{-1} from average lifetime and quantum yield data (Barkley et al., 1986), the recovered $k_{oi} = 1.1 \times 10^8$ s^{-1} gives $k_{isc} = (3–6) \times 10^7$ s^{-1}. This intersystem crossing rate is a little lower than the 8×10^7 s^{-1} value estimated from low-temperature luminescence yields in ethanol (Barkley et al., manuscript in preparation). The activation energies determined from lifetime data agree well with the 23 kJ/mol value derived from quantum yield data (Barkley et al., 1991).[2]

Bonding Kinetics. The rate of formation of tomaymycin–DNA adduct was measured at 5° intervals from 5 to 25 °C. At each temperature, fluorescence lifetime data were acquired at 313-nm excitation and 420-nm emission wavelengths as a function of time after mixing tomaymycin and DNA. The set of decay curves from the kinetics experiment and a free drug decay curve were fit to a triple exponential by global analysis. Figure 6 shows the time course of the relative amplitudes of the free drug component and the two DNA adduct components at 10 °C. The amplitude of each species is proportional to its concentration. The rate constants for the formation of DNA adducts were calculated assuming pseudo-first-order kinetics. Table 3 gives the apparent bimolecular rate constants measured at 10 °C, along with the Arrhenius parameters for the bonding reaction. The rate of formation of the longer lifetime species is faster than that of the shorter lifetime species. Drug binding usually involves positive entropy changes, presumably due to the release of ordered water from DNA to bulk solvent (Breslauer et al., 1987; Barkley et al., 1991). The negative $\Delta S^{\ddagger}$ values suggest that the water molecules remain in the transition state for the formation of tomaymycin–DNA adduct.

[2] The 18 kJ/mol activation energy reported previously was determined from the temperature dependence of the quantum yield, assuming that k_r was the only temperature-independent rate (Barkley et al., 1991). Use of $k_o = 1.1 \times 10^8$ s^{-1} to generate the Arrhenius plot gives $E_a = 23$ kJ/mol.

DISCUSSION

For tomaymycin–DNA adduct at low bonding density, the preferred lifetime model is a double exponential. The reasons are as follows: (1) the experimental data were fit equally well by distribution and double-exponential models; (2) the fit was not improved when more components were considered in the discrete analysis; (3) the standard deviations in the bimodal Gaussian distribution (0.13–0.23 ns) and the dispersions in the MEM amplitude profile (0.55–0.75 ns) were small; (4) probably most importantly, the MEM analysis of a biexponential decay simulated with the same parameters as the biexponential analysis of the experimental data gave the same two peaks as the experimental data; and (5) the dispersions of the peaks obtained from MEM analyses of simulated and experimental data were similar. When the DNA is saturated with tomaymycin, the fluorescence decay data no longer fit a double-exponential model and the lifetime model becomes a bimodal distribution. The reasons are as follows: (1) the fit was improved by increasing the number of discrete components up to three; (2) only two peaks were recovered from Gaussian and MEM analyses; and (3) simulation studies of discrete and Gaussian distribution models supported a bimodal distribution. In practice, it is impossible to distinguish lifetime distributions from closely spaced multiple discrete lifetimes (Siemiarczuk et al., 1990). Given the possibility of 64 bonding species, a distribution is plausible in tomaymycin–DNA adduct at high bonding density.

Because MEM analysis of time-resolved fluorescence data is still relatively new (Siemiarczuk & Ware, 1989; Gentin et al., 1990; Royer et al., 1990; Fetler et al., 1992), we comment briefly on its performance in our hands. Apparently, MEM could separate two discrete lifetimes as close together as 2.5 ns with the ratio $\tau_2/\tau_1 \geq 1.5$ (Figure 5). Tomaymycin–DNA adduct has two lifetimes separated by 2.8 ns with $\tau_2/\tau_1 = 1.65$ (Table 1). However, these lifetime differences and ratios are higher than the reported 2 ns and $\tau_2/\tau_1 = 1.4$ (Livesey & Brochon, 1987). Our failure to match the published resolution is due to lower counts in our data. The data collected by Brochon and co-workers using a synchrotron light source have 5–8 times better counting statistics than our data. Simulation results showed that about 1.5×10^5 counts in the peak channel are required to achieve the reported resolution. Unfortunately, it is impractical to acquire data of such high precision with a picosecond dye laser excitation source. On the other hand, dispersion values are relatively insensitive to the number of counts. For two discrete lifetimes of 4.3 and 7.1 ns, the dispersions decreased from 0.55 and 0.75 ns to 0.35 and 0.48 ns, with a 20-fold increase in counts in the peak channel from 3.6×10^4 to 7.2×10^5. Thus, it appears impossible to distinguish a lifetime distribution with 0.5-ns dispersion from a discrete model for these two peaks.

Natural sequence DNAs contain all 16 possible DNA bonding sites. At the low bonding density (140 nucleotides per drug) used in our experiments, one drug is bonded per 70 base pairs or one per 23 bonding sites, assuming a three base pair site. Under these conditions, tomaymycin will bond preferentially at the 5′-PuGPu sequence (Hertzberg et al., 1986; Hurley et al., 1988; Pierce et al., 1993). Detailed sequence specificity has been investigated by two footprinting techniques: exonuclease III stop assay (Hurley et al., 1988) and UvrABC incision analysis (Pierce et al., 1993). The results are similar but not identical, presumably due to the differences in DNA restriction fragments, reaction conditions, and detection levels. For example, the fragment used in the exonuclease III study lacks three possible bonding sites: 5′-AGA, 5′-GGG, and 5′-TGC. Two of these, 5′-AGA and 5′-TGC, are among the most frequently modified sites in the UvrABC incision analysis. Tomaymycin favors the 5′-AGA site by at least a factor of 3 over other bonding sites. The calf thymus DNA sample used in the fluorescence experiments has a length of more than 12 000 base pairs, which provides a random collection of bonding sites. Tomaymycin–DNA adducts are equilibrated for 2 or more weeks, allowing the drug to locate preferred sites. Thus, there is probably only one or at least a predominant species, owing to the sequence preference of adduct formation.

So far, 7 of the 16 bonding sites have been examined by fluorescence in adducts containing unique sites (Cheatham et al., 1988; Boyd et al., 1990; Barkley et al., manuscript in preparation). Only one or two species are present on each sequence. The poly(dA–dG)·poly(dC–dT) adduct with a 5′-AGA bonding site has decay parameters whose 4.8- and 7.2-ns lifetimes with relative amplitudes of 0.37 and 0.63 (Barkley et al., manuscript in preparation) are similar to those of the calf thymus DNA adduct. Two other bonding sites, 5′-GGG and 5′-CGC, have 7-ns lifetimes (Barkley et al., manuscript in preparation). The 5′-GGG site has a single lifetime, whereas 5′-CGC has a second lifetime of 5.0 ns with a relative amplitude of 0.17. We propose that the two species of DNA adduct at low bonding density represent mostly the 5′-AGA site. This agrees with the sequence specificity determined by UvrABC incision analysis. Purine–pyrimidine tracts, up to 100 base pairs in length, are frequently found in the 5′-flanking regions of eukaryotic genes, representing up to 1% of the genome (Hoffman-Liebermann et al., 1986). The S1-nuclease hypersensitivity of these tracts suggests that they adopt unusual conformations to regulate gene transcription (Wells, 1988). The strong preference of pyrrolo[1,4]benzodiazepines for homopurine sites points to regulatory regions of the DNA as a likely biological target.

The fluorescence lifetime depends more strongly on the binding mode than on the flanking base sequence (Barkley et al., manuscript in preparation). We propose that the major species of DNA adduct with the longer lifetime is the *S*3′ adduct, and the minor species with the shorter lifetime is the *R*5′ adduct. The binding mode at three sites has been determined by NMR studies of oligonucleotide adducts (Cheatham et al., 1988; Boyd et al., 1990; Wang et al., 1992). Two of these sites, 5′-TGC (Cheatham et al., 1988) and 5′AGC (Barkley et al., manuscript in preparation), have two fluorescent species with lifetimes of about 2.5 and 5.5 ns; the 5′-CGA site has a single lifetime of 6.4 ns (Boyd et al., 1990). NMR assigns the 6-ns-lifetime species to the *S*3′ adduct. The minor 2.5-ns-lifetime species was identified as the *R*5′ adduct at the 5′-TGC site by NMR. The 5′-AGA, 5′-GGG, 5′-TGT and 5′-CGC bonding sites in polynucleotide adducts likewise have a single or major component of 5.3–7.2-ns lifetime, which we assign to the *S*3′ binding mode (Barkley et al., manuscript in preparation). The minor species with 3.1–5-ns lifetime probably represents the *R*5′ binding mode. However, NMR studies suggest that tomaymycin may also form an *S*5′ adduct (Wang et al., 1992). More NMR studies of oligonucleotide adducts will be necessary to determine the binding mode of these minor species.

Tomaymycin saturates calf thymus DNA when there is one drug bonded per 8–9 base pairs or one per 2–3 potential bonding sites (Barkley et al., manuscript in preparation). If we assume random DNA sequences, one-third to one-half of the 16 bonding sites would be occupied. The lifetimes of DNA adducts at unique bonding sites cluster in two groups: a minor component of 1.5–5 ns and a major component of 5–8 ns (Barkley et al., manuscript in preparation). The amplitude

profile from MEM analysis suggests that all of these species may be present on the natural DNA sequence. On the other hand, the bimodal Gaussian results suggest that the longer discrete lifetime of 6.6 ns may represent *S*3′ adducts at 5′-AGA, 5′-GGG, and 5′-CGC sequences with the shorter broad lifetime distribution corresponding to the rest of the bonding species. However, the lifetimes of adducts at specific bonding sites may change at high bonding density due to distortion of the DNA. Finally, the bimodal distributions at high bonding density are probably not contaminated by free drug because all samples were extracted four times, kept at or below 5 °C, and discarded <12 h after extraction, during which time dissociation of the adduct is negligible.

Tomaymycin is buried in the minor groove of the DNA helix, with the 8-hydroxyl group pointing away from the DNA core. The fluorescence intensity of the DNA adduct prepared at P/D = 100 is invariant from pH 6.5 to 10.5 (Barkley et al., 1991). Thus, we expect and observe the fluorescence decay parameters to be independent of pH over the same range. Low molecular weight DNA fragments appear to have a larger fraction of minor species. This may be related to the DNA conformational change presumed to limit the bonding reaction in high molecular weight DNAs (Kizu et al., 1993; Barkley et al., manuscript in preparation). Relaxation of distortion through the ends of the molecule may allow the formation of a larger percentage of the less favored species.

Excited-state proton transfer appears to be the major environmentally sensitive nonradiative process in tomaymycin (Chen & Barkley, 1994). Presumably, it accounts for the temperature dependence of the fluorescence lifetimes of DNA adducts. The frequency factors of 1.1×10^{12} and 3.5×10^{11} s^{-1} and activation energy of 21 kJ/mol are comparable to values reported for intermolecular excited-state proton-transfer reactions: 7.2×10^{10} s^{-1} and 15 kJ/mol in 3-methylindole (Yu et al., 1992); 8.1×10^{12} s^{-1} and 17 kJ/mol in naphthylammonium ion 18-crown-6 complexes (Shizuka et al., 1985); and for the intramolecular excited-state proton transfer in tryptamine, 3.8×10^{11} s^{-1} and 17 kJ/mol (Shizuka et al., 1988). The proton-transfer rate depends on the proximity of proton donors or acceptors to tomaymycin in the DNA adduct. As suggested by molecular modeling studies of the tomaymycin–d(ATGCAT)$_2$ adduct, different binding modes have different hydrogen-bonding patterns between tomaymycin and DNA bases and water molecules in the minor groove (Barkley et al., 1991). The hydrogen-bonding pattern may be responsible for the different frequency factors in the two adducts.

REFERENCES

Arora, S. K. (1981) *J. Antibiot. 34*, 462–464.

Barkley, M. D., Cheatham, S., Thurston, D. E., & Hurley, L. H. (1986) *Biochemistry 25*, 3021–3031.

Barkley, M. D., Thomas, T. J., Maskos, K., & Remers, W. A. (1991) *Biochemistry 30*, 4421–4431.

Beechem, J. M. (1989) *Chem. Phys. Lipids 50*, 237–251.

Boyd, F. L., Stewart, D., Remers, W. A., Barkley, M. D., & Hurley, L. H. (1990) *Biochemistry 29*, 2387–2403.

Breslauer, K. J., Remeta, D. P., Chou, W.-Y., Ferrante, R., Curry, J., Zaunczkowski, D., Snyder, J. G., & Marky, L. A. (1987) *Proc. Natl. Acad. Sci. U.S.A. 84*, 8922–8926.

Cheatham, S., Kook, A., Hurley, L. H., Barkley, M. D., & Remers, W. (1988) *J. Med. Chem. 31*, 583–590.

Chen, Q., & Barkley, M. D. (1994) *J. Am. Chem. Soc.* (submitted for publication).

Fetler, L., Tauc, P., Hervé, G., Ladjimi, M. M., & Brochon, J.-C. (1992) *Biochemistry 31*, 12504–12513.

Gentin, M., Vincent, M., Brochon, J.-C., Livesey, A. K., Cittanova, N., & Gallay, J. (1990) *Biochemistry 29*, 10405–10412.

Gull, S. F., & Skilling, J. (1984) in *Indirect Imaging* (Roberts, J. A., Ed.) pp 267–279, Cambridge University Press, Cambridge, U.K.

Hertzberg, R. P., Hecht, S. M., Reynolds, V. L., Molineux, I. J., & Hurley, L. H. (1986) *Biochemistry 25*, 1249–1258.

Hoffman-Liebermann, B., Lieberman, D., Troutt, A., Kedes, L. H., & Cohen, S. N. (1986) *Mol. Cell. Biol. 6*, 3632–3642.

Hurley, L. H. (1977) *J. Antibiot. 30*, 349–370.

Hurley, L. H., & Needham-VanDevanter, D. R. (1986) *Acc. Chem. Res. 19*, 230–237.

Hurley, L. H., Reck, T., Thurston, D. E., Langley, D. R., Holden, K. G., Hertzberg, R. P., Hoover, J. R. E., Gallagher, G., Jr., Faucette, L. F., Mong, S.-M., & Johnson, R. K. (1988) *Chem. Res. Toxicol. 1*, 258–268.

Jaynes, E. T. (1983) in *Papers on Probability, Statistics and Statistical Physics* (Rosenkrantz, R. D., Ed.) pp 210–314, D. Reidel, Dordrecht, The Netherlands.

Kizu, R., Draves, P., & Hurley, L. H. (1993) *Biochemistry 32*, 8712–8722.

Kolber, Z. S., & Barkley, M. D. (1986) *Anal. Biochem. 152*, 6–21.

Livesey, A. K., & Skilling, J. (1985) *Acta Crystallogr. A41*, 113–122.

Livesey, A. K., & Brochon, J.-C. (1987) *Biophys. J. 52*, 693–706.

McMahon, L. P., Colucci, W. J., McLaughlin, M. L., & Barkley, M. D. (1992) *J. Am. Chem. Soc. 114*, 8442–8448.

Petrusek, R. L., Anderson, G. L., Garner, T. F., Fannin, Q. L., Kaplan, D. J., Zimmer, S. G., & Hurley, L. H. (1981) *Biochemistry 20*, 1111–1119.

Pierce, J. R., Nazimiec, M., & Tang, M.-S. (1993) *Biochemistry 32*, 7069–7078.

Remers, W. A., Barkley, M. D., & Hurley, L. H. (1992) in *Nucleic Acid Targeted Drug Design* (Propst, C. L., & Perun, T. J., Eds.) pp 375–422, Marcel Dekker, New York.

Royer, C. A., Gardner, J. A., Beechem, J. M., Brochon, J.-C., & Matthews, K. S. (1990) *Biophys. J. 58*, 363–378.

Shizuka, H., Kameta, K., & Shinozaki, T. (1985) *J. Am. Chem. Soc. 107*, 3956–3963.

Shizuka, H., Seizawa, M., Kobayashi, H., Kameta, K., Sugiyama, H., Matsuura, T., & Saito, I. (1988) *J. Am. Chem. Soc. 110*, 1726–1732.

Siemiarczuk, A., & Ware, W. R. (1989) *J. Phys. Chem. 93*, 7609–7618.

Siemiarczuk, A., Wagner, B. D., & Ware, W. R. (1990) *J. Phys. Chem. 94*, 1661–1666.

Skilling, J., & Bryan, R. K. (1984) *Mon. Not. R. Astron. Soc. 211*, 111–124.

Stryjewski, W. J. (1991) *Rev. Sci. Instrum. 62*, 1921–1925.

Wang, J.-J., Hill, G. C., & Hurley, L. H. (1992) *J. Med. Chem. 35*, 2995–3002.

Wells, R. D. (1988) *J. Biol. Chem. 263*, 1095–1098.

Yu, H.-T., Colucci, W. J., McLaughlin, M. L., & Barkley, M. D. (1992) *J. Am. Chem. Soc. 114*, 8449–8454.